ISSN 1674-1056
http://cpb.iphy.ac.cn
http://iopscience.iop.org/cpb
中国物理 B
Chinese Physics
中国物理 Chinese Physics B

Three-mode optomechanical system for angular velocity detection

Kai Li(李凯), Sankar Davuluri, Yong Li(李勇)

Citation: Chin. Phys. B . 2018, 27(8): 084203. **doi:** 10.1088/1674-1056/27/8/084203

Journal homepage: http://cpb.iphy.ac.cn; http://iopscience.iop.org/cpb

What follows is a list of articles you may be interested in

Multi-window transparency and fast-slow light switching in a quadratically coupled optomechanical system assisted with three-level atoms

Wan-Ying Wei(魏晚迎), Ya-Fei Yu(於亚飞), Zhi-Ming Zhang(张智明)

Chin. Phys. B . 2018, 27(3): 034204. **doi:** 10.1088/1674-1056/27/3/034204

Effect of radiation-induced color centers absorption in optical fibers on fiber optic gyroscope for space application

Jing Jin(金靖), Ya Li(李亚), Zu-Chen Zhang(张祖琛), Chun-Xiao Wu(吴春晓), Ning-Fang Song(宋凝芳)

Chin. Phys. B . 2016, 25(8): 084213. **doi:** 10.1088/1674-1056/25/8/084213

Electromagnetically induced transparency in a three-mode optomechanical system

Yan Xiao-Bo, Gu Kai-Hui, Fu Chang-Bao, Cui Cui-Li, Wu Jin-Hui

Chin. Phys. B . 2014, 23(11): 114201. **doi:** 10.1088/1674-1056/23/11/114201

Review of cavity optomechanical cooling

Liu Yong-Chun, Hu Yu-Wen, Wong Chee Wei, Xiao Yun-Feng

Chin. Phys. B . 2013, 22(11): 114213. **doi:** 10.1088/1674-1056/22/11/114213

Enhancing stationary optomechanical entanglement with Kerr medium

Zhang Dan, Zhang Xiao-Ping, Zheng Qiang

Chin. Phys. B . 2013, 22(6): 064206. **doi:** 10.1088/1674-1056/22/6/064206

Three-mode optomechanical system for angular velocity detection*

Kai Li(李凯), Sankar Davuluri, and Yong Li(李勇)†

Beijing Computational Science Research Center, Beijing 100193, *China*

(Received 12 April 2018; revised manuscript received 21 May 2018; published online 10 July 2018)

We propose a scheme for measuring the angular velocity of absolute rotation using a three-mode optomechanical system in which one mode of the two-dimensional (2D) mechanical resonator is coupled to an optical cavity. When the total system rotates, the Coriolis force acting on the 2D mechanical resonator due to the absolute rotation will affect the mechanical motion and thus change the phase of the output field from the cavity. The angular velocity of the absolute rotation can be estimated by monitoring the spectrum of the output field from the cavity via homodyne measurement. The minimum measurable angular velocity, which is determined by the noise spectrum, is calculated. The working range of the gyroscope for measuring angular velocity is discussed.

Keywords: optomechanics, gyroscope

PACS: 42.50.Lc, 06.30.Gv, 42.50.–p **DOI:** 10.1088/1674-1056/27/8/084203

1. Introduction

Inertial navigation[1,2] systems have many applications such as guiding missiles, satellites, and so on. At a fundamental level, an inertial navigation system contains an accelerometer, which is used to measure instantaneous velocity, and a gyroscope which plays an important role as a direction sensor. Different kinds of gyroscopes like mechanical gyroscopes [e.g., gyroscopes based on microelectromachanical systems (MEMSs)[3,4] utilizing the Coriolis force], optical gyroscopes (e.g., ring-laser gyroscopes and fiber-optic gyroscopes, which utilize the Sagnac effect,[5]) and nuclear magnetic resonance gyroscopes[6,7] or atom interferometer gyroscopes[8,9] which utilize the quantum effect, have been studied extensively.

On the other hand, because of the recent advances in nano-fabrication techniques for designing high-quality optical and mechanical resonators, optomechanics has emerged as a rapidly developing field for exploring the coupling between optical fields and mechanical oscillations. One of the most promising applications of optomechanics is for designing highly sensitive optical detection of small forces,[10–13] displacements[14–17] or masses[18–20] by manipulating the mechanical motion of a macroscopic object in the quantum regime.[21–28] Hence, optomechanical systems are used to detect the angular velocity of absolute rotation,[29] by optically monitoring the Coriolis force acting on the two-dimensional (2D) mechanical resonator.

Gyroscopes based on the Coriolis force detection were discussed in Refs. [3] and [29]. The analysis provided in Ref. [29] is based on classical mechanics and the effects of quantum noise, such as optomechanical back-action noise, are neglected. Recently, we presented theoretical analysis for the application of the optomechanical cavities for absolute rotation detection[30–32] by considering the effects of shot noise, back-action noise, and thermal noise.[33] In this work, we propose an optomechanical gyroscope model, where one mode of the 2D mechanical resonator is coupled to an optical cavity. Our model is similar to that in Refs. [31] and [32] except that here we do not use an external drive on the mechanical resonator. A strong external mechanical drive used in previous optomechanical gyroscopes[29,31,32] and thus the driven mode of the 2D mechanical resonator is treated classically by ignoring the effects of the related thermal noise and Coriolis force. In the present work, without using such an external drive, we treat all the three-modes of the system quantum mechanically and provide an alternative method for measuring angular velocity.

2. Model and Hamiltonian

The gyroscope is made of a three-mode optomechanical system, shown in Fig. 1(a), consisting of two parts: a 2D mechanical oscillator which does simple harmonic motion along the x axis and y axis, and a single-mode cavity field which is used to monitor the 2D mechanical oscillator's displacement along the x axis via optomechanical coupling of the radiation pressure force. The gyroscope is placed on a platform rotating with angular velocity Ω. Ω is along the z axis and goes through the original point, e.g., the center of the platform.

In the coordinate system fixed to the rotating platform,

*Project supported by the National Key Research and Development Program of China (Grant No. 2016YFA0301200), the National Basic Research Program of China (Grant No. 2014CB921403), the Science Challenge Project of China (Grant No. TZ2017003), and the National Natural Science Foundation of China (Grant Nos. 11774024, 11534002, and U1530401).

†Corresponding author. E-mail: liyong@csrc.ac.cn

© 2018 Chinese Physical Society and IOP Publishing Ltd

the Hamiltonian of the 2D mechanical oscillator is given as

$$H_m = \frac{m}{2}\left(\omega_x^2 x^2 + \omega_y^2 y^2\right) + \frac{1}{2m}[(p_x + m\Omega y)^2 + (p_y - m\Omega x)^2], \quad (1)$$

where x and y represent the displacements of the mechanical oscillator along the x axis and y axis, respectively. m and ω_x (ω_y) are the mass and the frequency of the mechanical oscillator along the x axis (y axis), respectively. The equilibrium position of the mechanical oscillator is placed at the original point. The terms depending on Ω in Eq. (1) result from the Coriolis force acting, in the x–y plane, on the 2D mechanical oscillator.

Noteworthily, we have omitted the centrifugal force in Eq. (1) by assuming it is much smaller than the Coriolis force, that is $m\Omega^2\sqrt{x^2+y^2} \ll 2m\Omega\sqrt{\dot{x}^2+\dot{y}^2}$. Actually, even though the centrifugal force is not negligible compared with the Coriolis force, it will also not bring a significant effect on our result of angular velocity detection. As we will show later, e.g., in Eqs. (31)–(39), the angular velocity is deduced by detecting the optical output spectrum. Though the Coriolis force will change the output spectrum in all the frequency range, we only focus on the spectrum around $\omega = \omega_y$ for a realistic detection. In contrast, the centrifugal force will only change the zero-frequency component of the output spectrum (for a constant angular velocity) and thus will not affect the detection result of angular velocity. For the sake of simplicity, we do not take the centrifugal force into account in this work.

The canonical momenta conjugate to x and y are given as[34,35]

$$p_x = m\dot{x} - m\Omega y, \quad p_y = m\dot{y} + m\Omega x, \quad (2)$$

where $m\dot{x}$ and $m\dot{y}$ represent the mechanical momenta of the mechanical oscillator along the x axis and y axis, respectively. Hence, the corresponding commutation relations are $[x, p_x] = \mathrm{i}\hbar$ and $[y, p_y] = \mathrm{i}\hbar$ with $\hbar$ the reduced Planck constant.

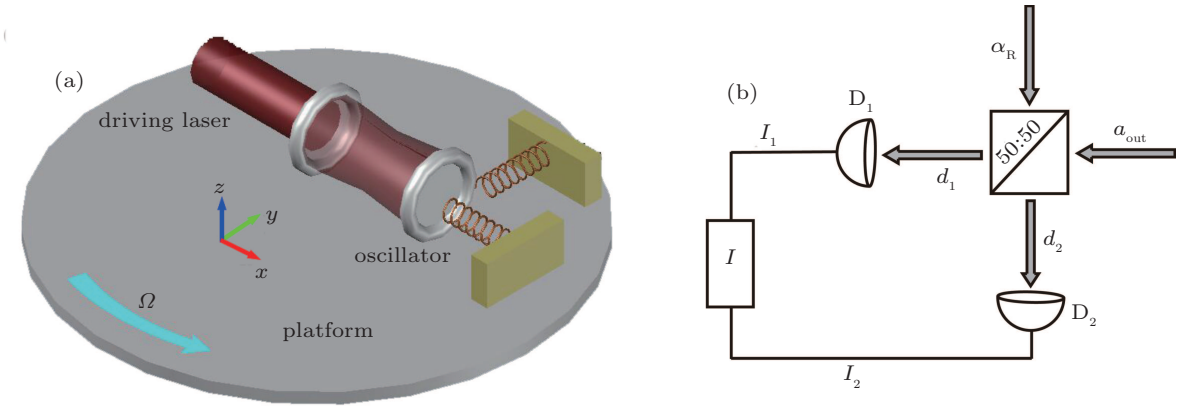


Fig. 1. (color online) (a) Schematics of the gyroscope containing the three-mode optomechanical system. A 2D mechanical oscillator (without mechanical drive) is placed on a platform rotating with angular velocity Ω (Ω is parallel to the z axis). The two mechanical modes are coupled by the Coriolis effect due to the absolute rotation. The mechanical motion in the x direction is coupled to an optical cavity by radiation pressure. (b) Schematics of the balanced homodyne measurement. The output field from the cavity is mixed with a much stronger classical reference laser at the input of a 50:50 beam splitter. The output from the beam splitter is fed to two photo-detectors D_1 and D_2. The difference in the photodetector readings gives the phase of the output field from the cavity.

The model under consideration is a three-mode optomechanical system involving two mechanical modes and one cavity field mode. After taking the cavity field into account, the Hamiltonian for the whole system is given as

$$H = H_m + \hbar(\omega_c + gx)a^\dagger a + \mathrm{i}\hbar\sqrt{2\kappa}\left(\bar{a}_{in}a^\dagger \mathrm{e}^{-\mathrm{i}\omega_d t} - \bar{a}_{in}^* a\,\mathrm{e}^{\mathrm{i}\omega_d t}\right), \quad (3)$$

where a is the annihilation operator for the cavity field, and $g = \omega_c/L$ is the single-photon radiation pressure coupling strength with L the length of the cavity and ω_c the eigenfrequency of the cavity. The cavity is coupled to an external driving field whose frequency and the driving strength are given as ω_d and $\sqrt{2\kappa}\bar{a}_{in}$, respectively.

After making a rotating frame at drive frequency ω_d, the Heisenberg–Langevin equations of motion are given as

$$\dot{x} = \frac{1}{m}(p_x + m\Omega y), \quad (4)$$

$$\dot{y} = \frac{1}{m}(p_y - m\Omega x), \quad (5)$$

$$\dot{p}_x = -m\omega_x^2 x + \Omega(p_y - m\Omega x) - \hbar g a^\dagger a - \gamma_x(p_x + m\Omega y) + \xi_x, \quad (6)$$

$$\dot{p}_y = -m\omega_y^2 y - \Omega(p_x + m\Omega y) - \gamma_y(p_y - m\Omega x) + \xi_y, \quad (7)$$

$$\dot{a} = -\mathrm{i}(\Delta_0 + gx)a - \kappa a + \sqrt{2\kappa}(\bar{a}_{in} + \delta a_{in}) \quad (8)$$

with κ being the decay rate of the cavity field and γ_x (γ_y) being the decay rate of the mechanical oscillation along the x axis (y axis). $\Delta_0 = \omega_c - \omega_d$ is the detuning between the cavity field mode and the drive field. $\xi_{x,y}$ and δa_{in} are the noise operators with zero mean values, and their non-zero correlations[36,37]

are given as

$$\left\langle \delta a_{\rm in}(t)\delta a_{\rm in}^{\dagger}(t')\right\rangle = \delta(t-t'), \tag{9}$$

$$\left\langle \xi_{x,y}(t)\xi_{x,y}(t')\right\rangle \approx 2m\gamma_{x,y}k_{\rm B}T\delta(t-t'), \tag{10}$$

where $k_{\rm B}$ is the Boltzmann constant and T is the bath temperature. We assumed that $k_{\rm B}T \gg \hbar\omega_{x,y}$ in Eq. (10).

Note that the present optomechanical gyroscope model is different from the ones used in previous works[29,31,32] in the following way. In the previous works,[29,31,32] a classical external drive is applied on the mechanical resonator along the y axis. In the presence of such a strong classical external drive, the mechanical motion along the y axis is treated classically (e.g., the classical motion with sinusoidal velocity[29,32] or constant velocity[31] along the y direction) by ignoring the effects of the related thermal noise and Coriolis force. Thus, the corresponding Heisenberg–Langevin equations of motion contain only a single cavity mode and a single mechanical mode in the x axis. In the present work, due to the absence of such a classical external drive in our model, the Heisenberg–Langevin equations of motion for the complete system includes the motion of all the three modes (one cavity mode and two mechanical modes) as given in Eqs. (4)–(8).

3. The spectrum of fluctuation and homodyne measurement

Equations (4)–(8) can be linearized by writing all the operators as $A = \bar{A} + \delta A$ ($A = a, x, y, p_x, p_y$), where $\bar{A}$ and δA are the classical mean value and quantum fluctuation of A. Thus the steady state solutions for the mean value equations of motion of Eqs. (4)–(8) can be obtained by setting $\mathrm{d}\bar{A}/\mathrm{d}t = 0$ as

$$\bar{x} = \frac{-\hbar g\,|\bar{a}|^2}{m\omega_x^2}, \quad \bar{y} = 0, \tag{11}$$

$$\bar{p}_x = 0, \quad \bar{p}_y = \frac{-\hbar g\Omega\,|\bar{a}|^2}{\omega_x^2}, \tag{12}$$

$$\bar{a} = \frac{\sqrt{2\kappa}\bar{a}_{\rm in}}{{\rm i}\Delta + \kappa}, \tag{13}$$

where the effective detuning is

$$\Delta = \Delta_0 + g\bar{x}. \tag{14}$$

As can be seen from Eq. (13), the mean photon number, which is given by $|\bar{a}|^2$, inside the cavity is independent of Ω. Hence we cannot estimate Ω by monitoring the mean intensity of the cavity output field. Thus, we shall focus on the equations of motion of the fluctuation operators in order to measure Ω. When $\Omega \neq 0$, the Coriolis force coupling between the two mechanical modes modifies the spectrum of the fluctuations in the output optical field via radiation-pressure optomechanical coupling. Thus the absolute rotation of the platform can be monitored from the spectrum of the fluctuations in the output optical field.

The linearized equations of motion for the fluctuation operators in Eqs. (4)–(8) are

$$\delta\dot{x} = \frac{1}{m}(\delta p_x + m\Omega\delta y), \tag{15}$$

$$\delta\dot{y} = \frac{1}{m}(\delta p_y - m\Omega\delta x), \tag{16}$$

$$\delta\dot{p}_x = -m\omega_x^2\delta x + \Omega\,(\delta p_y - m\Omega\delta x) - \hbar G\left(\delta a + \delta a^{\dagger}\right) - \gamma_x(\delta p_x + m\Omega\delta y) + \xi_x, \tag{17}$$

$$\delta\dot{p}_y = -m\omega_y^2\delta y - \Omega(\delta p_x + m\Omega\delta y) - \gamma_y(\delta p_y - m\Omega\delta x) + \xi_y, \tag{18}$$

$$\delta\dot{a} = -{\rm i}\Delta\delta a - {\rm i}G\delta x - \kappa\delta a + \sqrt{2\kappa}\delta a_{\rm in}, \tag{19}$$

where the effective coupling strength $G = g\bar{a}$ has been assumed to be real without loss of generality. Note that in writing Eqs. (15)–(19), the higher-order terms like $\delta x\delta a$ are neglected. This is reasonable since we can make $|\bar{a}| \gg 1$ by changing the intensity of the driving laser, $\bar{a}_{\rm in}$.

By defining the Fourier transform of operator A as

$$\tilde{A}(\omega) = \int_{-\infty}^{+\infty} {\rm e}^{{\rm i}\omega t}A(t)\,\mathrm{d}t$$

with $\tilde{A}^{\dagger}(\omega) = \left[\tilde{A}(-\omega)\right]^{\dagger}$, we obtain the solution to the linearized equations (15)–(19) in the frequency domain as

$$\delta\tilde{a}(\omega) = \chi_1(\omega)\tilde{a}_{in}(\omega) + \chi_2(\omega)\tilde{a}_{in}^{\dagger}(\omega) + \chi_3(\omega)\tilde{\xi}_x(\omega) + \chi_4(\omega)\tilde{\xi}_y(\omega) \tag{20}$$

with

$$\chi_1(\omega) = \frac{\sqrt{2\kappa}}{\eta^*(-\omega)}[\hbar G^2\chi_y(\omega)\chi(\omega)\eta(\omega) - 1], \tag{21}$$

$$\chi_2(\omega) = \sqrt{2\kappa}\hbar G^2\chi(\omega)\chi_y(\omega), \tag{22}$$

$$\chi_3(\omega) = G\eta(\omega)\chi(\omega)\chi_y(\omega), \tag{23}$$

$$\chi_4(\omega) = 2\omega\Omega G\eta(\omega)\chi(\omega). \tag{24}$$

Here we defined

$$\chi_{x,y}(\omega) = \gamma_{x,y}\omega - {\rm i}(\omega^2 - \omega_{x,y}^2),$$

$$\eta(\omega) = {\rm i}(\omega + \Delta) - \kappa,$$

$$[\chi(\omega)]^{-1} = 2{\rm i}G^2\hbar\Delta\chi_y(\omega) - m\eta(\omega)\eta^*(-\omega)\cdot[\chi_x(\omega)\chi_y(\omega) + 4\omega^2\Omega^2].$$

Making use of the input–output relationship[38] $a_{\rm out} + a_{\rm in} = \sqrt{2\kappa}a$, we can obtain the fluctuation and steady-state mean value of the output cavity field as

$$\delta a_{\rm out} = \sqrt{2\kappa}\delta a - \delta a_{\rm in}, \tag{25}$$

$$\bar{a}_{\rm out} = \frac{\kappa - {\rm i}\Delta}{\kappa + {\rm i}\Delta}\bar{a}_{\rm in} \tag{26}$$

with $a_{\rm in} \equiv \bar{a}_{\rm in} + \delta a_{\rm in}$ and $a_{\rm out} \equiv \bar{a}_{\rm out} + \delta a_{\rm out}$.

The phase of the output field, represented by $a_{\rm out}$, from the cavity is measured using a homodyne setup as shown in Fig. 1(b). The output field $a_{\rm out}$ is mixed with a classical reference laser field,[39] whose amplitude is $\alpha_{\rm R}$, at a 50:50 beam splitter as shown in Fig. 1(b). The output from the beam splitter is fed onto photo-detectors D_1 and D_2. The readings in D_1 and D_2 are given as $d_1^\dagger d_1$ and $d_2^\dagger d_2$, respectively, with $d_1 = (a_{\rm out} + {\rm i}\alpha_{\rm R})/\sqrt{2}$ and $d_2 = ({\rm i}a_{\rm out} + \alpha_{\rm R})/\sqrt{2}$. The difference in the photo detector readings is given as

$$I = I_1 - I_2 = {\rm i}\alpha_{\rm R}(a_{\rm out}^\dagger - a_{\rm out}), \tag{27}$$

where $\alpha_{\rm R}$ has been taken to be real.

We rewrite I as a sum of its mean value and fluctuation by writing $I \equiv \bar{I} + \delta I$. So we obtain

$$\bar{I} = {\rm i}\alpha_{\rm R}(\bar{a}_{\rm out}^* - \bar{a}_{\rm out}), \tag{28}$$

which is independent of Ω. The fluctuation δI in I is given as

$$\delta I = {\rm i}\alpha_{\rm R}(\delta a_{\rm out}^\dagger - \delta a_{\rm out}). \tag{29}$$

The spectrum of δI is given as

$$S_{\rm II}(\omega) = \int_{-\infty}^{+\infty} {\rm e}^{{\rm i}\omega t} \langle \delta I(t)\delta I(0)\rangle \, {\rm d}t. \tag{30}$$

By using Eqs. (9), (10), (20), (25), and (29), we can obtain the spectrum

$$S_{\rm II}(\omega) = |\bar{a}_{\rm R}|^2 [S_{\rm add}(\omega) + S_{xx}(\omega) + S_{yy}(\omega)] \tag{31}$$

with

$$S_{\rm add}(\omega) = \left|\{4\kappa\hbar G^2\chi_y(\omega) + 2\kappa m\eta(\omega)[\chi_x(\omega)\chi_y(\omega) + 4\omega^2\Omega^2]\}\chi(\omega) - 1\right|^2, \tag{32}$$

$$S_{xx}(\omega) = 16\kappa m\gamma_x k_{\rm B}T \left|G({\rm i}\omega - \kappa)\chi(\omega)\chi_y(\omega)\right|^2, \tag{33}$$

$$S_{yy}(\omega) = 64\kappa m\gamma_y k_{\rm B}T\Omega^2 |G\omega({\rm i}\omega - \kappa)\chi(\omega)|^2. \tag{34}$$

In Eq. (31), $S_{\rm add}$ includes both the optical shot noise and the optomechanical back-action noise, S_{xx} gives the thermal noise in the mechanical oscillator's motion along the x axis, and S_{yy} gives the effect of the Coriolis force on the mechanical oscillator's motion along the x axis due to the thermal vibrations along the y axis. Note that $\chi(\omega)$ is dependent on Ω, which means S_{xx} and S_{yy} (as well as $S_{\rm add}$) include the effect of the Coriolis forces.

4. Estimation of angular velocity and its minimum detectable value

In principle, the fact that all the three parts ($S_{\rm add}$, S_{xx}, and S_{yy}) in the spectrum $S_{\rm II}$ depend on Ω, allows one to measure Ω by monitoring the optical output spectrum. Here, we will just focus on the following simple case

$$|\chi_x(\omega)\chi_y(\omega)| \gg 4\omega^2\Omega^2. \tag{35}$$

When equation (35) is satisfied, $\chi(\omega)$ is independent of Ω and is given as

$$[\chi(\omega)]^{-1} = [2{\rm i}G^2\hbar\Delta - m\eta(\omega)\eta^*(-\omega)\chi_x(\omega)]\chi_y(\omega). \tag{36}$$

Thus, both $S_{\rm add}(\omega)$ and $S_{xx}(\omega)$ are independent of Ω, and $S_{yy}(\omega)$ can be rewritten as

$$S_{yy}(\omega) = \Omega^2\sigma^2(\omega) \tag{37}$$

with the transmission coefficient

$$\sigma(\omega) = 8\sqrt{\kappa m\gamma_y k_{\rm B}T}\,|G\omega({\rm i}\omega - \kappa)\chi(\omega)|. \tag{38}$$

The fact that S_{yy} is proportional to Ω^2 provides us with a method to estimate the angular velocity as $\Omega = \sqrt{S_{yy}(\omega)}/\sigma(\omega)$, from the homodyne measurement results of the optical output spectrum. The other two parts in the spectrum $S_{\rm II}(\omega)$, i.e., $S_{\rm add}$ and S_{xx}, determine the noise in the optical output spectrum. Hence the minimum measurable angular velocity $\Omega_{\rm noise}$ is given as

$$\Omega_{\rm noise}(\omega) = \frac{1}{\sigma(\omega)}\sqrt{S_{\rm add}(\omega) + S_{xx}(\omega)}. \tag{39}$$

In principle, the above minimum measurable angular velocity will be obtained when the measurement time $t_{\rm m} \to \infty$. Note that the signal spectrum $S_{yy}(\omega)$ as well as the transmission coefficient $\sigma(\omega)$ is a Lorentz peak with full width at half maximum being of the order of γ_y. In a realistic detection, when the measurement time is long enough such that $t_{\rm m} \gg 1/\gamma_y$, one can obtain approximately the minimum measurable angular velocity $\Omega_{\rm noise}$.

In what follows, we will only consider two limiting cases: $S_{\rm add}(\omega) \ll S_{xx}(\omega)$ and $S_{\rm add}(\omega) \gg S_{xx}(\omega)$.

When

$$S_{\rm add}(\omega) \ll S_{xx}(\omega), \tag{40}$$

the minimum detectable angular velocity

$$\Omega_{\rm noise}(\omega) \approx \frac{\sqrt{S_{xx}(\omega)}}{\sigma(\omega)} = \frac{|\gamma_y\omega - {\rm i}(\omega^2 - \omega_y^2)|}{2\omega}\sqrt{\frac{\gamma_x}{\gamma_y}} \tag{41}$$

is independent of T, Δ, and ω_x.

According to Eq. (41), $\Omega_{\rm noise}(\omega)$ reaches its minimum value $\sqrt{\gamma_x\gamma_y}/2$ when $\omega = \omega_y$. For simulation, we consider the parameters:[40] $m = 6.9 \times 10^{-4}$ kg, $\omega_y/2\pi = 84.8$ Hz, $\gamma_x/2\pi = \gamma_y/2\pi = 1.9 \times 10^{-3}$ Hz, $\kappa/2\pi = 4 \times 10^6$ Hz, and $g/2\pi = 1.46 \times 10^{17}$ Hz/m. Temperature is as $T = 300$ K and the effective optomechanical coupling strength is $G/2\pi = 2.19 \times 10^{22}$ Hz/m (with the corresponding $\bar{a} = 1.5 \times 10^5$). The minimum detectable angular velocity is shown in Fig. 2(a)

with the optimal value $\Omega_{\rm noise}(\omega_y)/2\pi = 9.5\times10^{-4}$ Hz. The corresponding transmission coefficient $\sigma(\omega_y)$ is optimized when $\Delta = 0$ as shown in Fig. 2(b).

Note that the above analysis for estimating the minimum detectable angular velocity as well as the optimal transmission coefficient is valid only when equations (35) and (40) are satisfied. As shown in Fig. 2(c), the condition in Eq. (35) is not fulfilled for the resonance case of $\omega_x = \omega_y$ when Ω is larger than the optimal minimum detectable angular velocity $\Omega_{\rm noise}$. For the non-resonance case of $\omega_x = 2\omega_y$ or $\omega_x = 0.5\omega_y$, the condition in Eq. (35) is satisfied well when $\Omega/2\pi$ is less than about 0.1 Hz ($\sim 10^{-3}\omega_y$). Since the condition of Eq. (40) is always fulfilled for the above parameters [see Fig. 2(d)], we can know that for the typical simulation parameters as given in the caption of Fig. 2 and the non-resonance case of $\omega_x \simeq 2\omega_y$, the optimal minimum detectable angular velocity of our optomechanical gyroscope is $\Omega_{\rm noise}(\omega_y)/2\pi = 9.5\times10^{-4}$ Hz with the corresponding working range of the angular velocity being $\Omega_{\rm noise}/2\pi \le \Omega/2\pi \lesssim 0.1$ Hz.

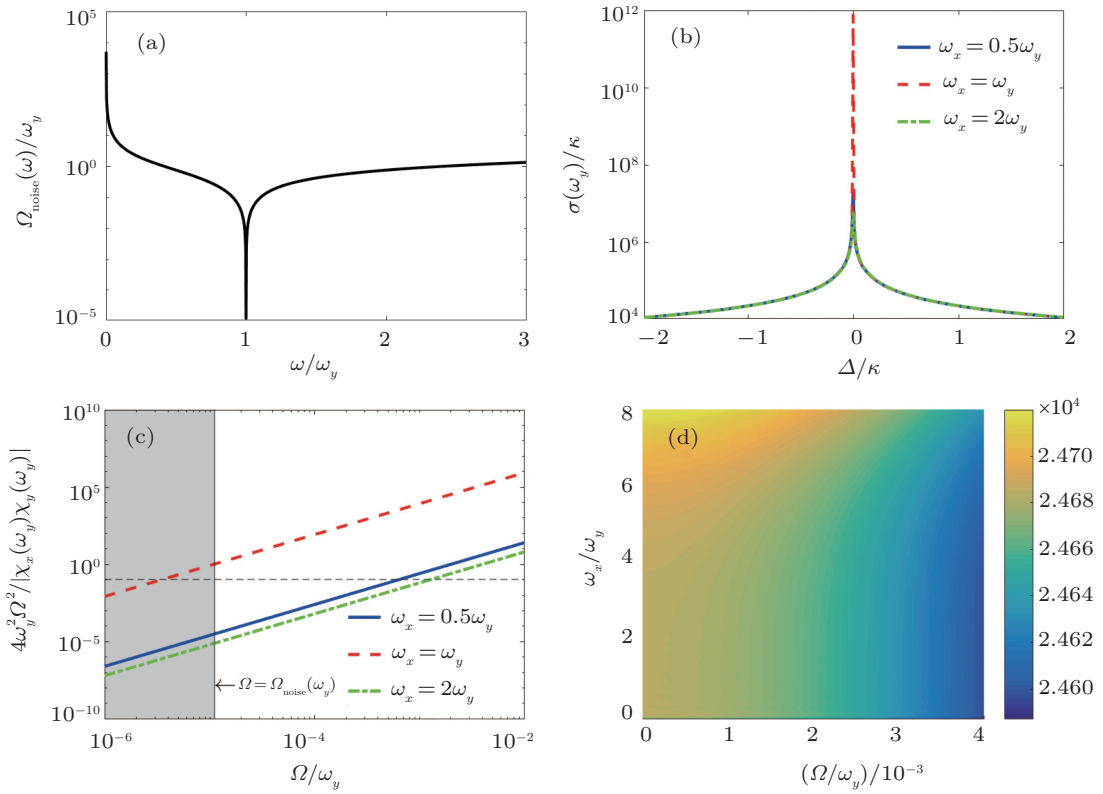


Fig. 2. (color online) (a) The minimum detectable angular velocity in Eq. (41). (b) The corresponding transmission coefficient $\sigma(\omega_y)$ versus Δ for different values of ω_x. (c) Simulation of the condition given in Eq. (35) with $\omega = \omega_y$ for different ω_x. (d) The ratio of $S_{\rm add}(\omega_y)$ in Eq. (32) to $S_{xx}(\omega_y)$ in Eq. (33) as a function of ω_x and Ω with fixed $\Delta = 0$ and $T = 300$ K. The other parameters are:[40] $m = 6.9\times10^{-4}$ kg, $\omega_y/2\pi = 84.8$ Hz, $\gamma_x/2\pi = \gamma_y/2\pi = 1.9\times10^{-3}$ Hz, $\kappa/2\pi = 4\times10^6$ Hz, and $g/2\pi = 1.46\times10^{17}$ Hz/m. The effective optomechanical coupling strength is taken as $G/2\pi = 2.19\times10^{22}$ Hz/m (with the corresponding $\bar{a} = 1.5\times10^5$). For these parameters, the optimal value of $\Omega_{\rm noise}(\omega_y)/2\pi = 9.5\times10^{-4}$ Hz, also see the vertical line in panel (c).

Now we consider the second limiting case: when

$$S_{\rm add}(\omega) \gg S_{xx}(\omega). \tag{42}$$

In this case the minimum detectable angular velocity reduces to

$$\Omega_{\rm noise}(\omega) \approx \frac{1}{\sigma(\omega)}\sqrt{S_{\rm add}(\omega)}, \tag{43}$$

which is dependent on T, Δ, and ω_x.

In Fig. 3(a), we plot the minimum detectable angular velocity in Eq. (43) for the parameters:[41] $m = 1.9\times10^{-7}$ kg, $\omega_y/2\pi = 8\times10^5$ Hz, $\gamma_x/2\pi = \gamma_y/2\pi = 80$ Hz, $\kappa/2\pi = 1\times10^6$ Hz, and $g/2\pi = 1.17\times10^{17}$ Hz/m. Temperature is $T = 300$ K and the effective optomechanical coupling strength is $G/2\pi = 3.51\times10^{20}$ Hz/m (with the corresponding $\bar{a} = 3\times10^3$). The optimal minimum detectable angular velocity appears at $\omega = \omega_y$ [as similar to the case in Fig. 2(a)] with $\Omega_{\rm noise}/2\pi = 92.6$ Hz, 40.0 Hz, and 336.4 Hz for $\omega_x = 0.5\omega_y$, ω_y, and $2\omega_y$, respectively. The corresponding transmission coefficient $\sigma(\omega_y)$ is shown in Fig. 3(b) with its optimal value appearing at $\Delta = 0$.

The above analysis of the minimum detectable angular velocity as well as the optimal transmission coefficient is only valid when equations (35) and (42) are satisfied. It is shown in Fig. 3(c) that the condition in Eq. (35) is not fulfilled for the resonance case of $\omega_x = \omega_y$ when Ω is larger than the optimal $\Omega_{\rm noise}$. However, this condition is satisfied well for the non-resonance case of $\omega_x = 2\omega_y$ or $\omega_x = 0.5\omega_y$ when $\Omega/2\pi$ is less than 800 Hz ($\sim 10^{-3}\omega_y$). It is shown in Fig. 3(d) that

the condition of Eq. (42) is always fulfilled for the above considered parameters. Thus we know for the typical parameters as given in the caption of Fig. 3, and under the non-resonance case $\omega_x \simeq 0.5\omega_y$, the optomechanical gyroscope works well when $\Omega_{\rm noise}(\omega_y)/2\pi \leq \Omega/2\pi \lesssim 800$ Hz and the optimal minimum detectable angular velocity $\Omega_{\rm noise}(\omega_y)/2\pi = 92.6$ Hz.

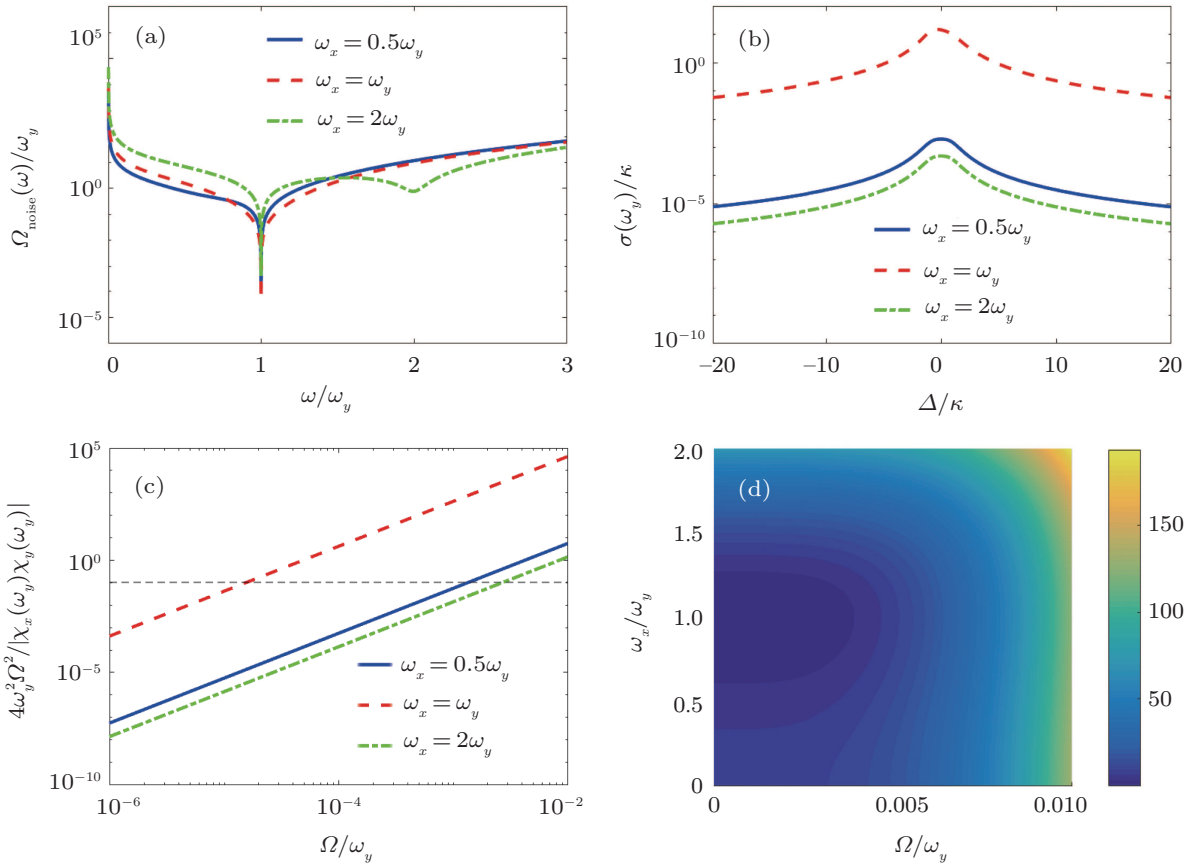


Fig. 3. (color online) (a) The minimum detectable angular velocity in Eq. (43) for different values of ω_x. (b) The corresponding transmission coefficient $\sigma(\omega_y)$ versus Δ for different ω_x. (c) Simulation of the condition given in Eq. (35) with $\omega = \omega_y$ for different ω_x. (d) The ratio of $S_{\rm add}(\omega_y)$ in Eq. (32) to $S_{xx}(\omega_y)$ in Eq. (33) as a function of ω_x and Ω. Here $\Delta = 0$ in panels (a) and (d). The other parameters are:[41] $m = 1.9 \times 10^{-7}$ kg, $\omega_y/2\pi = 8 \times 10^5$ Hz, $\gamma_x/2\pi = \gamma_y/2\pi = 80$ Hz, $\kappa/2\pi = 1 \times 10^6$ Hz, $T = 300$ K, and $g/2\pi = 1.17 \times 10^{17}$ Hz/m. The effective optomechanical coupling strength is taken as $G/2\pi = 3.51 \times 10^{20}$ Hz/m (with the corresponding $\bar{a} = 3 \times 10^3$).

5. Discussion and conclusion

In conclusion, we studied the application of a three-mode optomechanical system as a gyroscope for detecting absolute rotation. Our model of an optomechanical gyroscope, where a cavity field mode is coupled to one of the two mechanical modes of a 2D resonator, is similar to the previous ones[29–31] except that here we do not use any additional external mechanical drive on the mechanical resonator. When our optomechanical system is placed on a rotating platform, the mechanical oscillation modes of the 2D mechanical oscillator are coupled due to the Coriolis force. Using the Heisenberg–Lengivin equations of motion, the dynamics of all the three modes (one cavity field mode and two mechanical oscillator modes) are studied. The angular velocity of the absolute rotation is estimated by monitoring the spectrum of the output field from the cavity via homodyne measurement. The noises in the output spectrum, which determine the minimum detectable angular velocity, include the thermal noise of the mechanical oscillator (S_{xx}), and the additional noise ($S_{\rm add}$) from the optical shot noise and optomechanical back-action. We further analyzed the cases when $S_{xx} \gg S_{\rm add}$ and $S_{xx} \ll S_{\rm add}$, and estimated the optimal minimum detectable angular velocity. The corresponding working ranges of the angular velocity in these two cases are also discussed.

We would like to remark that our analysis is based on the condition in Eq. (35), which requires that the angular velocity should not be too strong. That is, the noises in the optical output spectrum are required to keep approximately unchanged when the system rotates. This limits the maximum value of the angular velocity to be detected in our model. Actually, similar conditions also exist in the previous optomechanical gyroscopes.[29,31,32] In future, we will further investigate the application of an optomechanical gyroscope in the case of large angular velocity which does not satisfy the condition in Eq. (35).

Acknowledgment

We would like to thank Prof. Peng Zhang, Prof. Hao Fu, and Dr. Wen-Zhao Zhang for their helpful discussions.

References

[1] Chatfield A B 2015 *Fundamentals of High Accuracy Inertial Navigation* (American Institute of Aeronautics and Astronautic)
[2] Britting K R 1971 *Inertial Navigation Systems Analysis* (Wiley-Interscience)
[3] Acar C and Shkel A 2009 *MEMS Vibratory Gyroscopes* (Spriger)
[4] Zaman M F, Sharma A, Hao Z and Ayazi F 2008 *Journal of Microelectromechanical System* **17** 1526
[5] Ezekiel S and Arditty H J 1981 *Fiber-Optic Rotation Sensors and Related Technologies* (Springer)
[6] Karwacki F A 1980 *Navigation* **27** 72
[7] Meyer D and Larsen M 2014 *Gyroscopy & Navigation* **5** 75
[8] Gustavson T L, Bouyer P and Kasevich M A 1997 *Phys. Rev. Lett.* **78** 2046
[9] Müller T, Gilowski M, Zaiser M, Berg P, Schubert Ch, Wendrich T, Ertmer W and Rasel E M 2009 *Eur. Phys. J. D* **53** 273
[10] The LIGO Scientific Collaboration 2013 *Nat. Photon.* **7** 613
[11] Rugar D, Budakian R, Mamin H J and Chui B W 2004 *Nature* **430** 329
[12] Zhang J Q, Li Y, Feng M and Xu Y 2012 *Phys. Rev. A* **86** 053806
[13] Xiong H, Si L G and Wu Y 2017 *Appl. Phys. Lett.* **110** 171102
[14] Hoff U B, Harris G I, Madsen L S, Kerdoncuff H, Lassen M, Nielsen B M, Bowen W P and Andersen U L 2013 *Opt. Lett.* **38** 1413
[15] Anetsberger G, Arcizet O, Gavartin E, Unterreithmeier Q P, Weig E M, Kotthaus J P and Kippenberg T J 2009 *Nat. Phys.* **5** 909
[16] Yin Z Q, Li T C and Feng M 2011 *Phys. Rev. A* **83** 013816
[17] Zhou L M, Xiao K W, Yin Z Q, Chen J and Zhao N 2017 arXiv: 1709.07177
[18] Lin Q, He B and Xiao M 2017 *Phys. Rev. A* **96** 043812)
[19] Li J J and Zhu K D 2012 *Appl. Phys. Lett.* **101** 141905
[20] Zhao N and Yin Z Q 2014 *Phys. Rev. A* **90** 042118
[21] Liao J Q and Law C K 2011 *Phys. Rev. A* **83** 033820
[22] Wang Q, Zhang J Q, Ma P C, Yao C M and Feng M 2015 *Phys. Rev. A* **91** 063827
[23] Xiong H, Si L G, Zheng A S, Yang X X and Wu Y 2012 *Phys. Rev. A* **86** 013815
[24] Wilson-Rae I, Nooshi N, Zwerger W and Kippenberg T J 2007 *Phys. Rev. Lett.* **99** 093901
[25] Guo Y J, Li K, Nie W J and Li Y 2014 *Phys. Rev. A* **90** 053841
[26] Fu H, Ding J F, Li Y and Cao G Y 2015 *Sci. China-Phys. Mech. Astron.* **58** 050304
[27] Zhang J, Mu Q X and Zhang W Z 2018 *Chin. Phys. B* **27** 040304
[28] Liu Y C, Xiao Y F, Luan X S and Wong C W 2015 *Sci. China-Phys. Mech. Astron.* **58** 050305
[29] Norgia M and Donati S Hybrid 2001 *Electron. Lett.* **37** 756
[30] Davuluri S 2016 *Phys. Rev. A* **94** 013808
[31] Davuluri S and Li Y 2016 *New J. Phys.* **18** 103047
[32] Davuluri S, Li K and Li Y 2017 *New J. Phys.* **19** 113004
[33] Gardiner C W and Zoller P 2000 *Quantum Noise* (Springer)
[34] Gazeau J P, Koide T and Murenzi R 2017 *Europhys. Lett.* **118** 50004
[35] Arnold V I, Kozlov V V and Neishtadt A I 2006 *Mathematical Aspects of Classical and Celestial Mechanics* (Springer)
[36] Breuer H P and Petruccione F 2006 *The theory of open quantum systems* (Oxford)
[37] Clerk A A, Devoret M H, Girvin S M, Marquardt F and Schoelkopf R J 2010 *Rev. Mod. Phys.* **82** 1155
[38] Walls D F and Milburn G J 2008 *Quantum Optics* (Springer)
[39] Loudon R and Knight P L 1987 *J. Mod. Opt.* **34** 709
[40] Mow-lowry C M, Mullavey A J, Gossler S, Gray M B and McClelland D E 2008 *Phys. Rev. Lett.* **100** 010801
[41] Arcizet O, Cohadon p -F, Briant T, Pinard M and Heidmann A 2006 *Nature* **444** 71